Supporting information

Covalent Organic Framework Derived Synthesis of Ru Embedded in Carbon Nitride for Hydrogen and Oxygen Evolution Reactions

Tianyu Gao[1#], Kilaparthi Sravan Kumar[2#], Zhen Yan[3], Maya Marinova[4], Martine Trentesaux[1], Mohammed A. Amin[5], Sabine Szunerits[2], Yong Zhou[1], Vlad Martin-Diaconescu[6], Sebastien Paul[1]*, Rabah Boukherroub[2]*, and Vitaly Ordomsky[1]*

[1]*Univ. Lille, CNRS, Centrale Lille, ENSCL, Univ. Artois, UMR 8181 – UCCS – Unité de Catalyse et Chimie du Solide, F-59000 Lille, France*

[2]*Univ. Lille, CNRS, Centrale Lille, Univ. Polytechnique Hauts-de-France, UMR 8520 - IEMN, F-59000 Lille, France*

[3]*E2P2L, UMI 3464 CNRS-Solvay, 3966 Jin Du Rd., 201108 Shanghai, China*

[4]*Univ. Lille, CNRS, INRAE, Centrale Lille, Univ. Artois, FR 2638 IMEC Institut Michel-Eugène Chevreul, F-59000 Lille, France*

[5]*Department of Chemistry, College of Science, Taif University, P.O. Box 11099, Taif 21944, Saudi Arabia*

[6]*ALBA Synchrotron – CELLS, Carrer de la Llum 2-26, 08290 Cerdanyola del Vallès Barcelona, Spain*

[#]*These two authors contributed equally to this work*

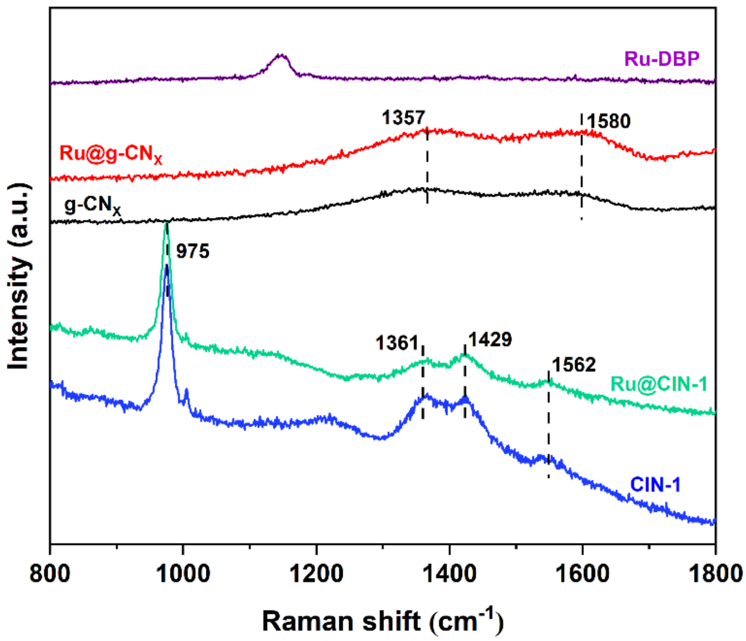

Figure S1. *Raman spectra of Ru-DBP, Ru@CIN-1, CIN-1, Ru@g-CN$_x$ and g-CN$_x$.*

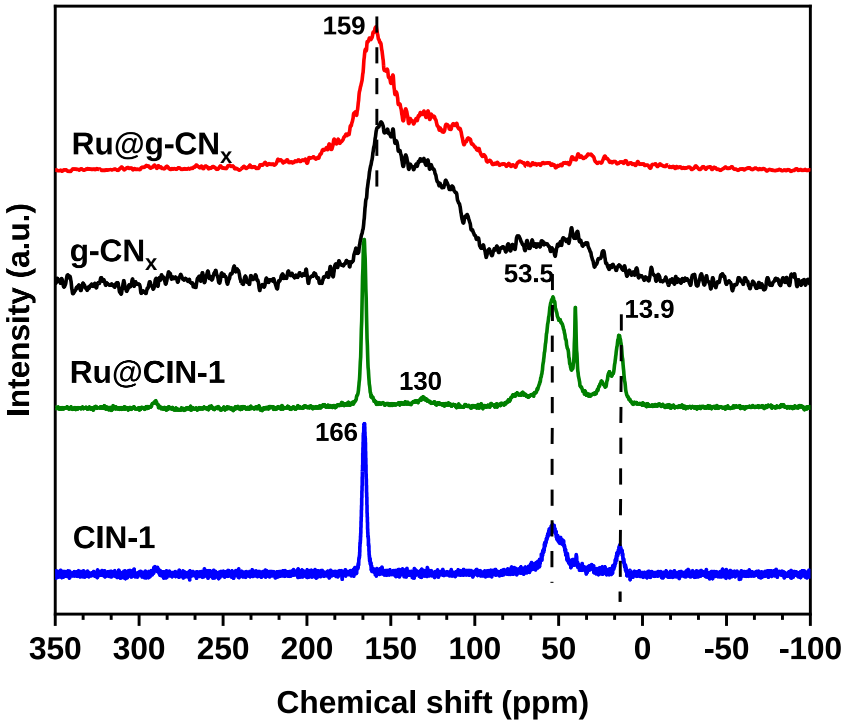

Figure S2. *^{13}C CP/MAS NMR spectra of CIN-1, Ru@CIN-1, Ru@g-CN$_x$ and g-CN$_x$.*

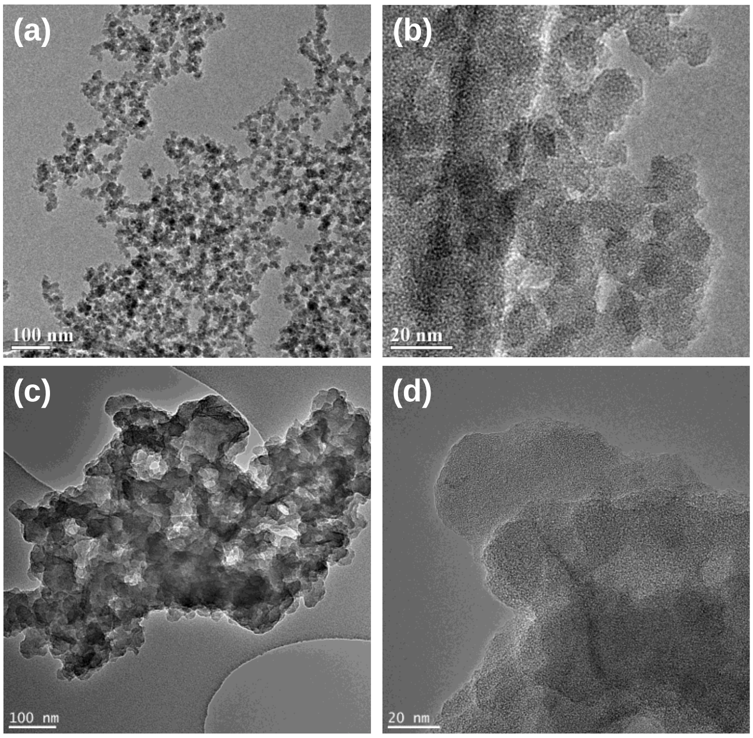

Figure S3. *TEM images of CIN-1 (a,b) and Ru@CIN-1 (c,d).*

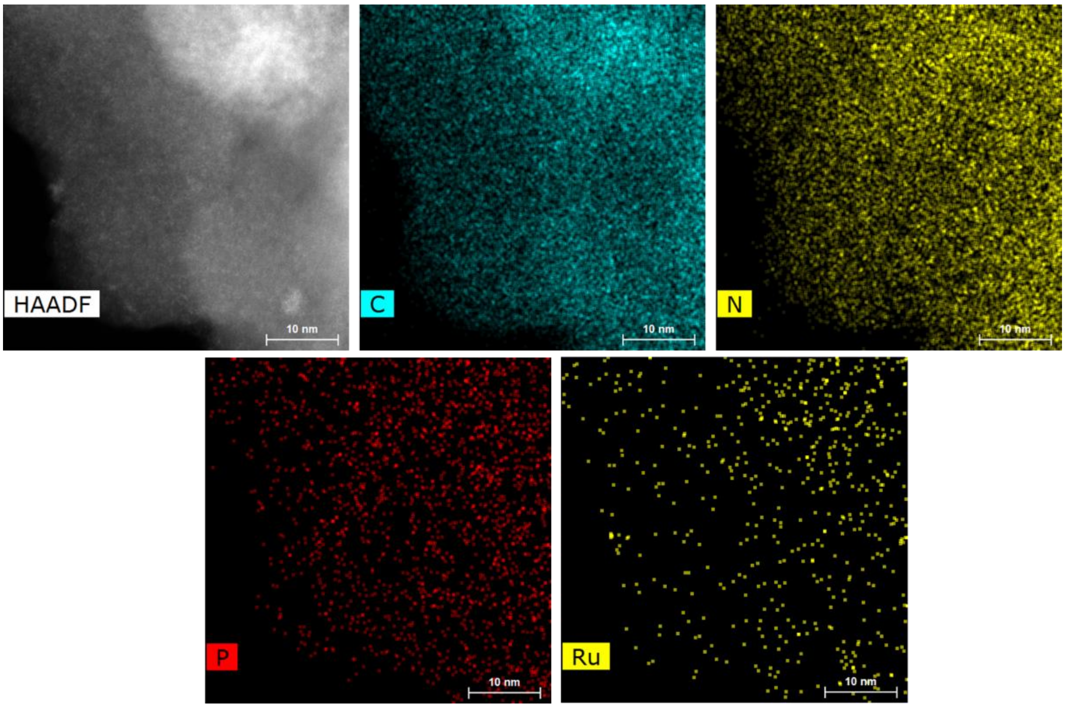

Figure S4. *Color-coded EDS elemental maps of C, N, P and Ru in the Ru@CIN-1 sample.*

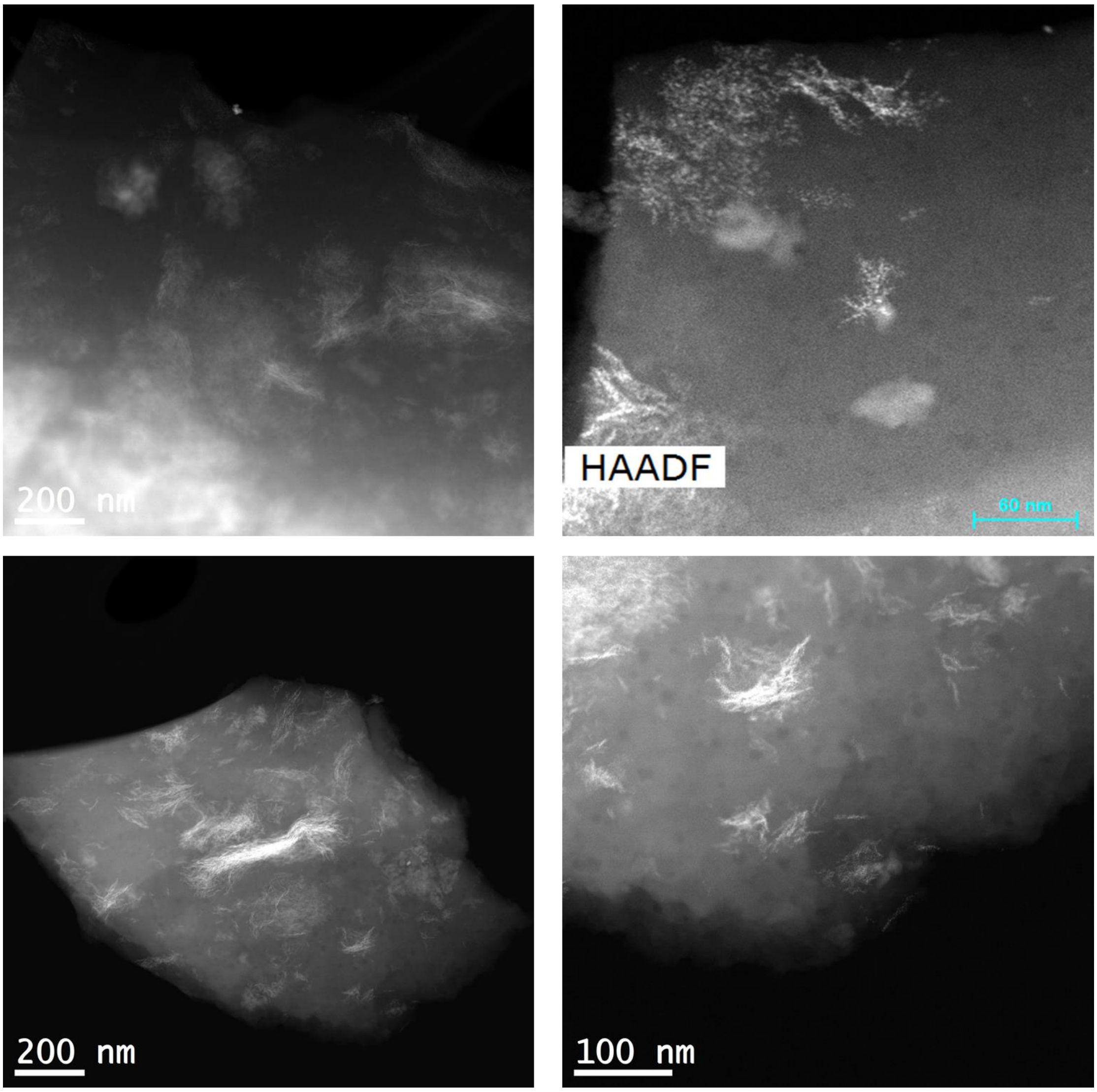

Figure S5. *STEM-HAADF images of Ru@g-CN$_X$*

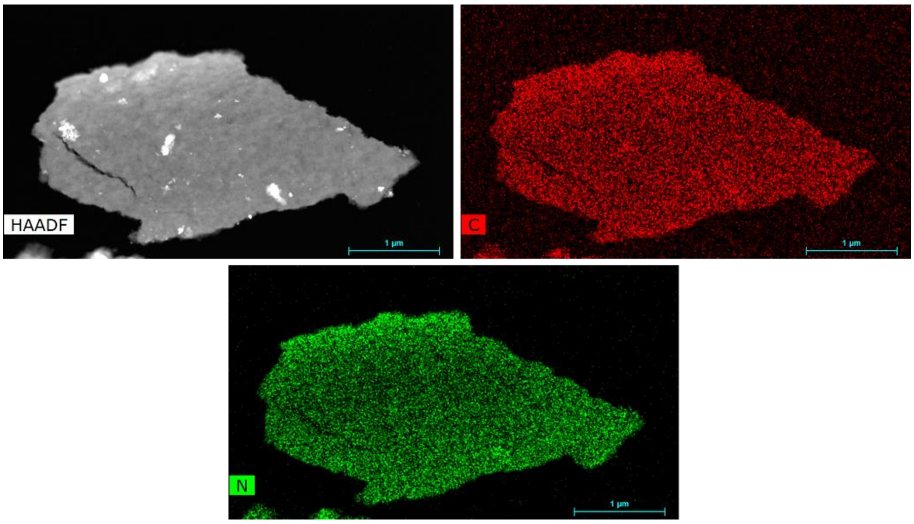

Figure S6. *STEM-HAADF of g-CN_X with EDS mapping of C and N.*

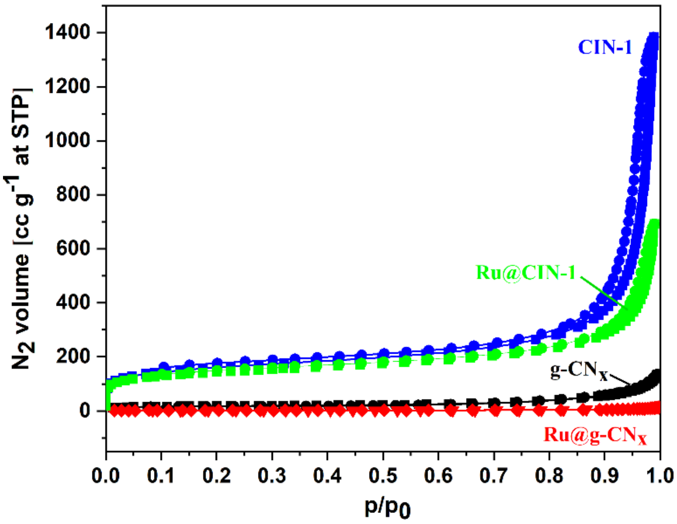

Figure S7. *N_2 adsorption-desorption isotherms of Ru@CIN-1, CIN-1, Ru@g-CN_x and g-CN_X.*

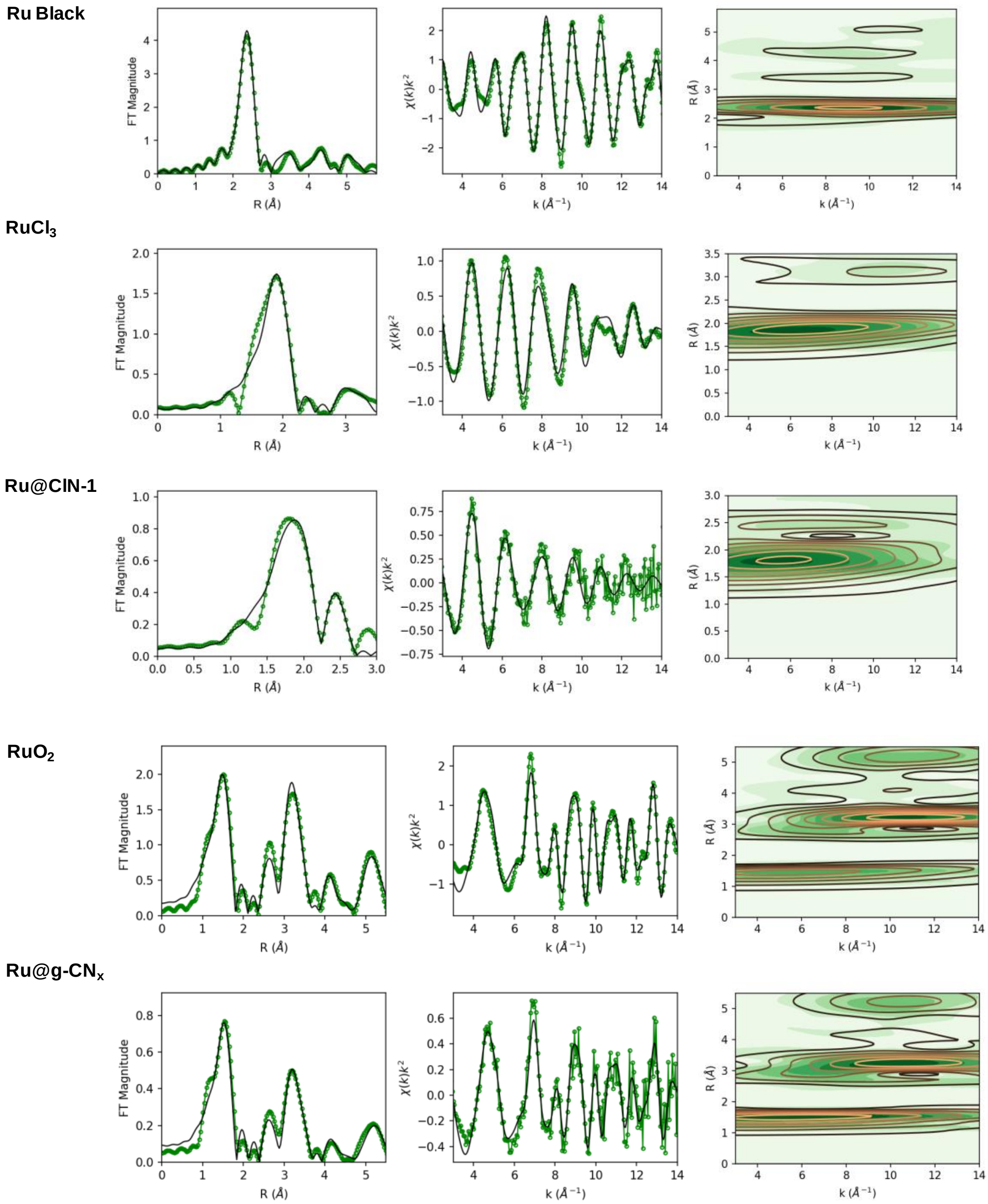

Figure S8. *EXAFS data (green) and fits (black) described in Table S1.*

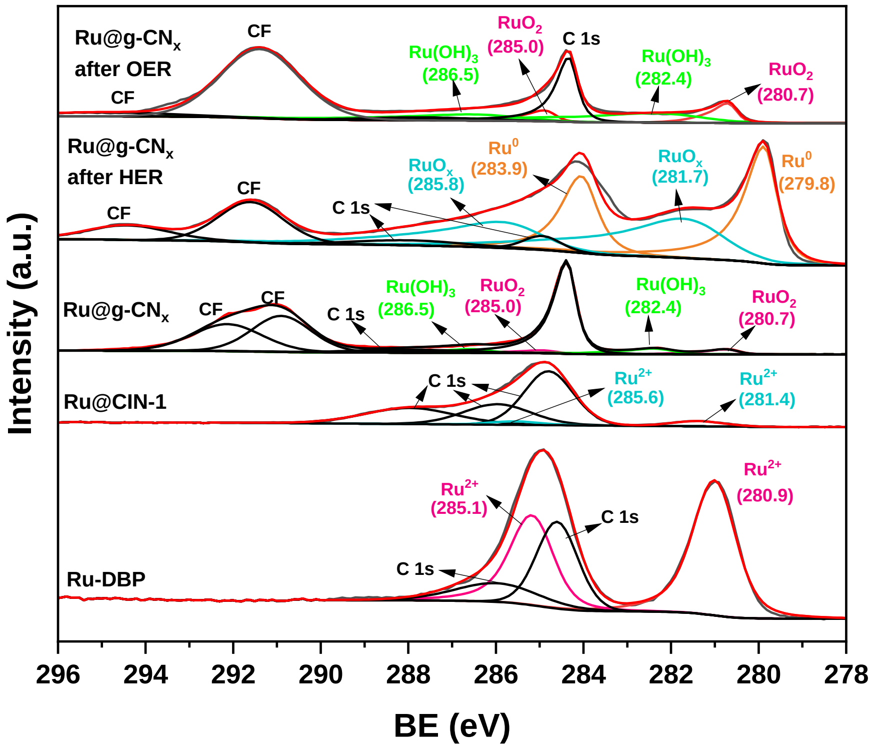

Figure S9. *XPS 3d Ru spectra of Ru-DBP, Ru@CIN-1, Ru@g-CN_x before and after HER and OER reaction*

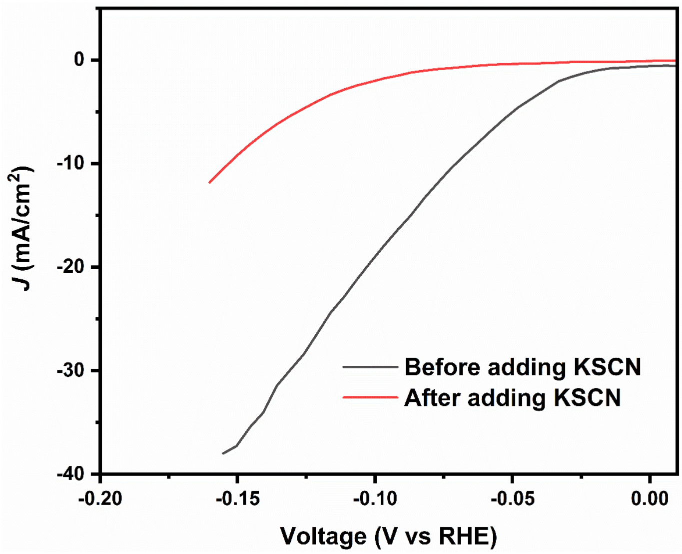

Figure S10. *LSV cathodic polarization curves of Ru@g-CN$_x$ in 1M KOH electrolyte solution before and after adding KSCN.*

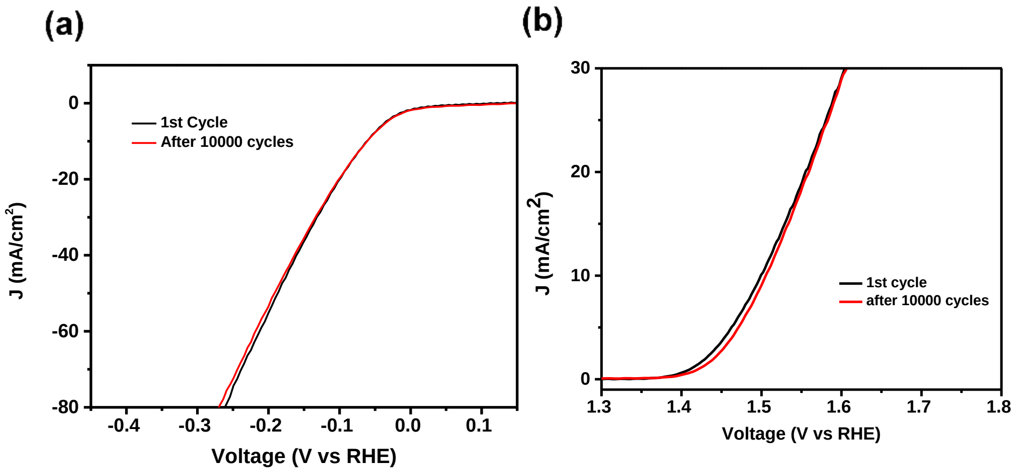

Figure S11. *HER (a) and OER (b) LSV polarization curves of Ru@g-CN$_x$ before and after 10000 CV cycles in 1M KOH*

Faradaic efficiency measurements for the HER and OER

In order to further assess its electrocatalytic performance toward both HE and OE reactions and support electrochemical results, faradaic efficiency (FE) measurements were also carried out on the best-performing catalyst, namely Ru@g-CN_x. This was accomplished by first using gas chromatography (GC) to quantify the volume of the gas expelled under the experimental conditions. The amount of the evolved H_2 is represented here as $V_{measured}$ and the experimental setup involved 1 h of controlled potentiostatic electrolysis (CPE) with the catalyst held at +1.0 V *vs.* RHE (for the OER) and -1.0 V *vs.* RHE (for the HER). Measurements were conducted in 1.0 M KOH solutions at 25 ^oC. Then, using the following ratio (1), the FE value was determined:

$$V_{measured}/V_{calculated} \quad (1)$$

where $V_{calculated}$ stands for the theoretical volume of the gas estimated from the charge passed through the working electrode during the employed CPE under the assumption of a 100% Faradaic efficiency.

For both the HER and OER, the Faradaic efficiency values were determined using the formula presented below[1]:

$$\text{Faradaic efficiency (\%)} = [F \times n \times mol\ gas\ (GC) \times 100]/Q(CPE)$$

Where Q(CPE) represents the charge transmitted through the WE during the controlled potential electrolysis (CPE), F is the Faraday's constant (F = 96485 C), mol gas (GC) denotes the volume of gas (either H_2 or O_2) released during the CPE and measured by GC. The parameter (n) represents the number of electrons transported during the HER (n = 2 for the reduction of H^+, $2H^+ + 2e^- = H_2$) and OER (n = 4 for the oxidation of OH^-, $4OH^- = 2H_2O + O_2 + 4e^-$). The Ru@g-$CN_x$ catalyst measured 31.8 mol H_2 (GC) for the HER, or 31.8×10^{-6} mol H_2 per hour, and the equivalent charge passed (Q) during the applied CPE was 6.15 C. Adding the values of mol H_2 (GC) and Q to the previous equation results in:

Faradaic efficiency (%) = [(96485) × 2 × (31.8 × 10^{-6}) × 100] / 6.15 = 99.78%

On the other hand, the Ru@g-CNx catalyst had a measured mol O_2 (GC) value for the OER of 16.28 × 10^{-6} mol h^{-1}, and the corresponding charge passed (*Q*) during the employed CPE was estimated to be 6.3 C. Inputting the mol O_2 (GC) and *Q* values into the previous equation results in:

Faradaic efficiency (%) = [(96485) × 4 × (16.28 × 10^{-6}) × 100] / 6.3 = 99.73%

Under the same experimental conditions, the FE values of the Ru@g-CN_x catalyst (99.78 and 99.73% for the HER and OER, respectively) were higher than those predicted for the commercial Pt/C (98.9% for the HER) and RuO_2 (99.2% for the OER). These results attest to the Ru@g-CN_x catalyst's exceptional catalytic activity.

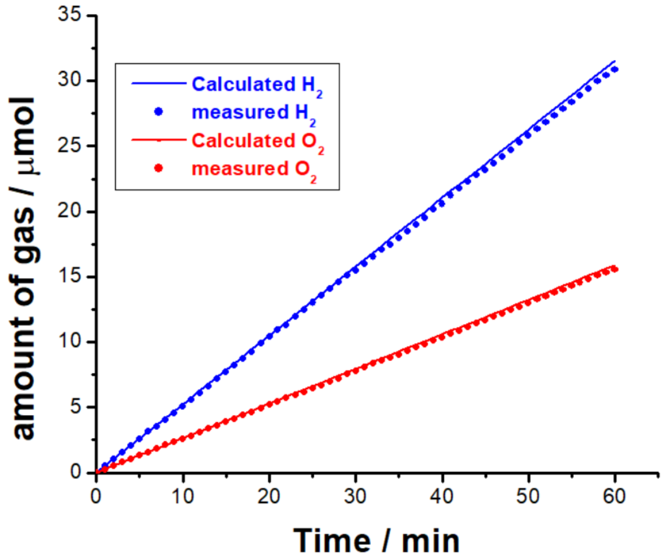

Figure S12. *Faradaic efficiency measurements for both HER and OER by the best performing catalyst (Ru@g-CN_x) in 1 M KOH. The electrode was held at -1.0 V vs. RHE (for the HER) and +1.0 V vs. RHE (for the OER) for 1 h in 1.0 M KOH solutions at 25 °C. The amount of the gas liberated expected from the amount of charge passed (6.15 and 6.3 C for HER and OER, respectively) assuming 100% Faradaic efficiency is shown as a solid line. The amount of the released gas detected by the GC is shown as solid spheres.*

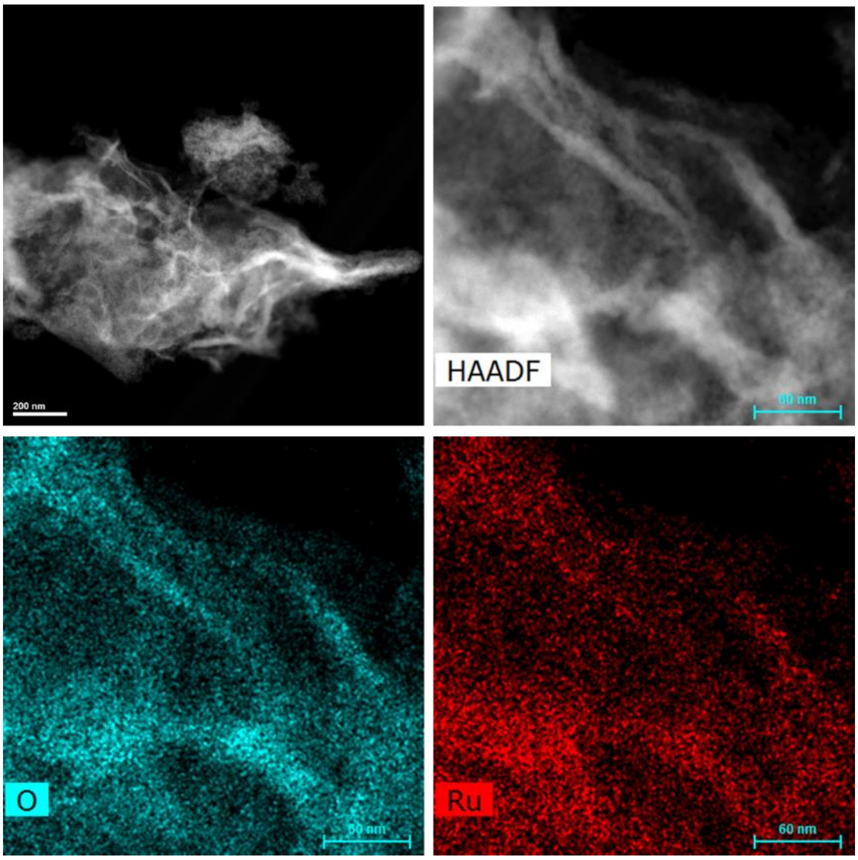

Figure S13. *STEM-HAADF image of Ru@g-CN_x catalyst after long term cathodic polarization with EDS mapping of Ru and O.*

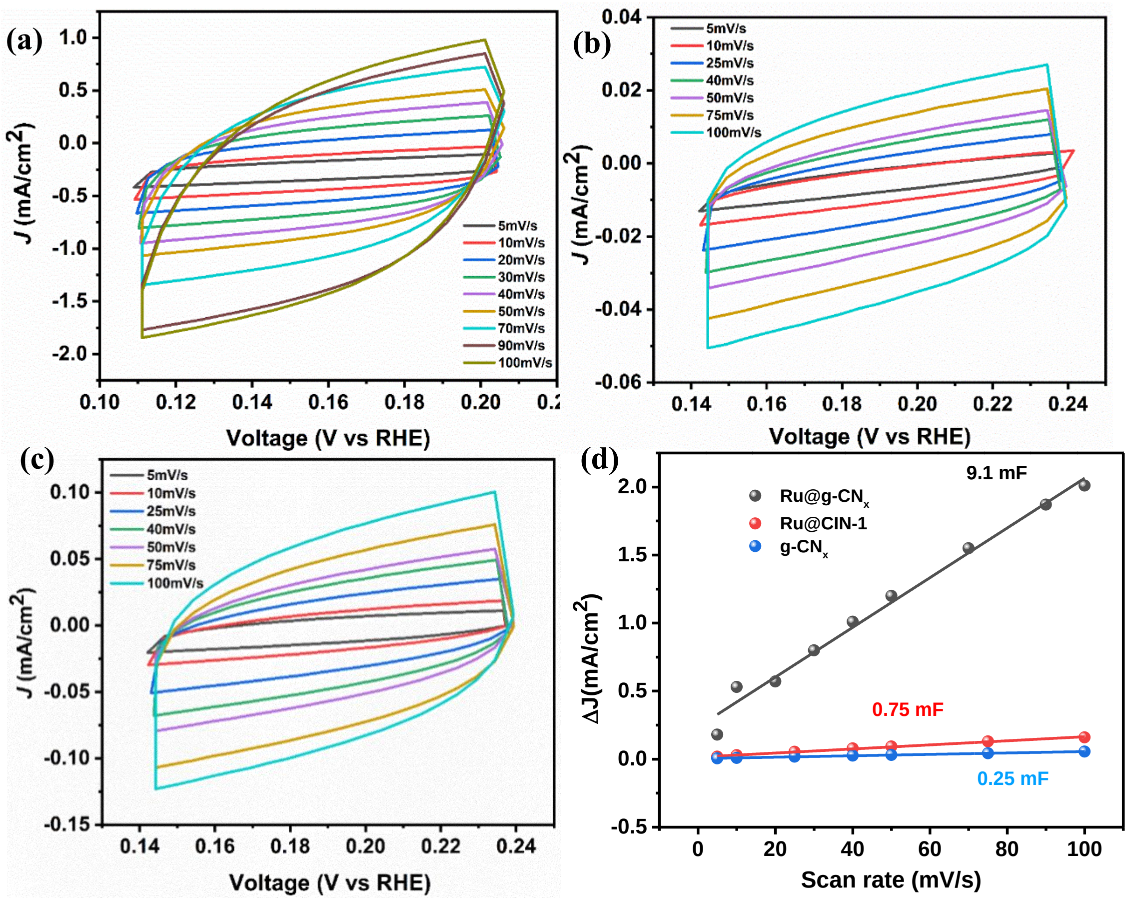

Figure S14. *(a) Cyclic voltammograms of (a) Ru@g-CN$_x$, (b) g-CN$_x$, and (c) Ru@CIN-1 in the 0.1 to 0.25 V vs RHE potential range. (d) Variation of the double layer charging currents at (a) 0.16V and (b,c) 0.19V vs scan rate*

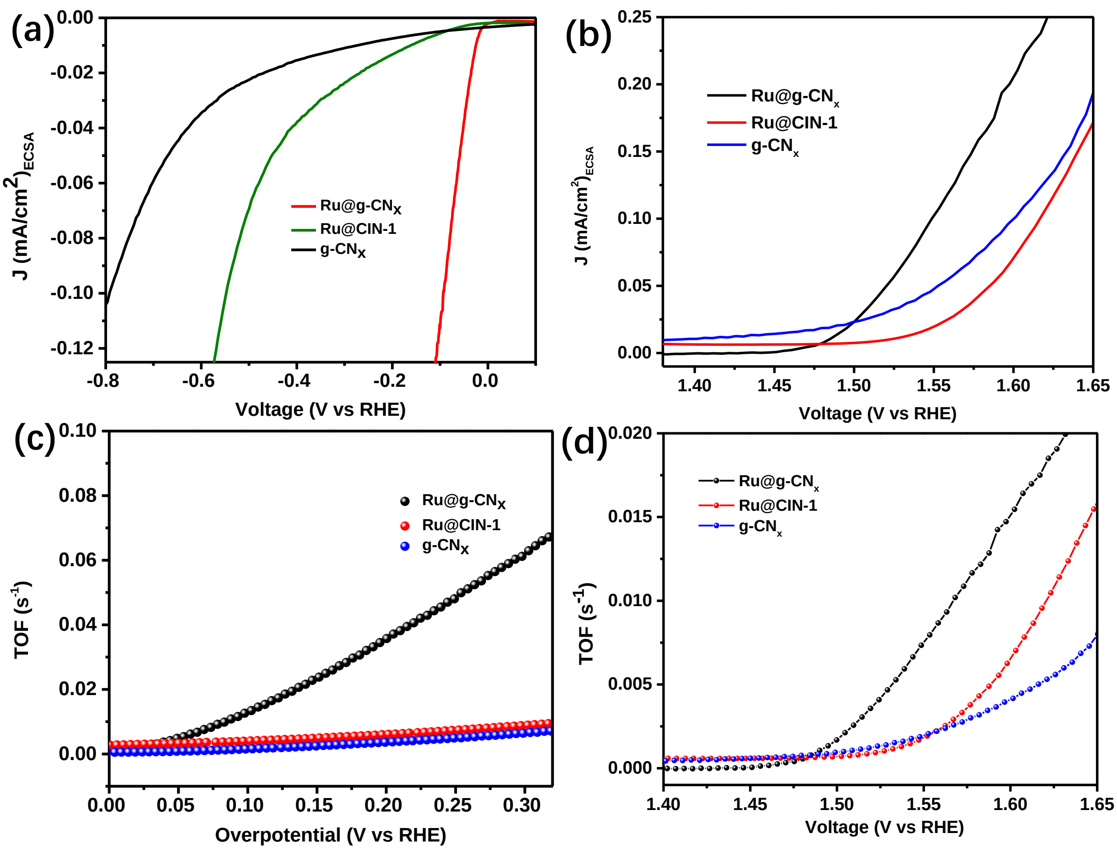

Figure S15. *ECSA-normalized LSV curves (a) HER polarization curves (b) OER polarization curves (c)TOF for HER polarization curves (d) TOF for OER polarization curves.*

Table S1. *Summary of EXAFS analysis. Multi (k^1, k^2, k^3)-weighted fits carried out in r-space over a k-range of 3-14 Å and an r-range as indicated, using a Hanning window (dk 1), and S_0 = 0.9. Bond distances and disorder parameters (Δr_{eff} and σ^2) were allowed to float having initial values of 0.0 Å and 0.003 Å^2 respectively, with a universal E_0 and ΔE_0 = 0 eV. (σ^2 reported as x10^3Å^2).*

Sample		Ru Black	$RuCl_3$	Ru@ClN-1
Δk		3-14	3-14	3-14
Δr		1-5.8	1-3.5	1-3.0
R_{FACTOR}		0.033	0.045	0.021
χ^2_v		1587	1067	6.1
ΔE_0		-5.2(0.6)	5.1(1.3)	6.0(1.7)
M-N/C/O	**N**		2	1.5
	r(Å)		2.24(0.02)	2.19(0.02)
	σ^2		3.8(0.8)	5.0(3.6)
M-P/Cl	**N**			1
	r(Å)			2.30(0.07)
	σ^2			5.0(3.6)
M-P/Cl	**N**		3	2
	r(Å)		2.37(0.01)	2.42(0.02)
	σ^2		3.8(0.8)	5.0(3.6)
M-Ru	**N**	12.0		1
	r(Å)	2.68(0.00)		2.70(0.02)
	σ^2	5.1(0.2)		6.2(1.7)
M-Ru	**N**	6.0	1	
	r(Å)	3.79(0.01)	3.39(0.02)	
	σ^2	5.9(0.8)	2.6(2.0)	
M-Ru	**N**	12.0		
	r(Å)	4.66(0.01)		
	σ^2	5.9(0.8)		
M-Ru	**N**	12.0		
	r(Å)	5.08(0.01)		
	σ^2	7.4(1.1)		
M - Ru - Ru	**N**	24.0		
	r(Å)	5.20(0.01)		
	σ^2	7.4(1.1)		
M - Ru - Ru	**N**	12.0		
	r(Å)	5.44(0.01)		
	σ^2	7.4(1.1)		
M - Ru - Ru - Ru	**N**	6.0		
	r(Å)	5.44(0.01)		
	σ^2	7.4(1.1)		

Sample		RuO2	Ru@g-CN_x
Δk		3-14	3-14
Δr		1.1-5.5	1.1-5.5
R_{FACTOR}		0.033	0.032
χ^2_v		1587	2.000
ΔE_0		-4.9(1.1)	3.0(0.8)
M-N/C/O	N	6.0	1.9
	r(Å)	1.97(0.00)	1.97(0.01)
	σ^2	2.5(0.5)	1.7(0.4)
M-Ru	N	2.0	0.6
	r(Å)	3.11(0.00)	3.11(0.00)
	σ^2	2.7(0.3)	3.1(0.3)
M-Ru	N	7.5	2.3
	r(Å)	3.55(0.00)	3.55(0.00)
	σ^2	2.7(0.3)	3.1(0.3)
M-O	N	4.0	-
	r(Å)	3.66(0.01)	-
	σ^2	3.9(1.3)	-
M-Ru-O	N	16.0	4.6
	r(Å)	3.73(0.01)	3.72(0.01)
	σ^2	3.9(1.3)	5.5(0.9)
M - O - Ru-O	N	2.0	0.6
	r(Å)	3.88(0.01)	5.5(0.9)
	σ^2	3.9(1.3)	4.0
M - O - Ru-O	N	4.0	1.2
	r(Å)	3.96(0.01)	3.96(0.01)
	σ^2	3.9(1.3)	5.5(0.9)
M - O	N	8.0	2.3
	r(Å)	4.03(0.01)	4.02(0.01)
	σ^2	3.9(1.3)	5.5(0.9)
M-Ru	N	4.0	1.2
	r(Å)	4.50(0.01)	4.49(0.01)
	σ^2	3.9(1.3)	5.5(0.9)
M-Ru	N	8.0	2.3
	r(Å)	5.47(0.01)	5.47(0.01)
	σ^2	4.6(0.6)	5.5(0.9)
M-Ru-O	N	16.0	4.6
	r(Å)	5.65(0.01)	5.65(0.01)
	σ^2	4.6(0.6)	5.5(0.9)

Table S2. *Comparison table of Ru based electrocatalysts for HER in 1M KOH*

Catalyst	Overpotential (At 10mA cm^{-2})	Tafel slope (mV dec^{-1})	Stability	References
Ru@C_2N	17	38	Not given	[2]
RuP_x@NPC	74	70	10 h	[3]
Ru_2P@PNC/CC-900	50	66	10 h	[4]
RuP2@NPC	52	69	10 h	[5]
$Ni_{1.5}Co_{1.4}P$@Ru	52	50	6 h	[6]
Ru/C	24	33	Not given	[7]
ah-RuO_2@C	63	62	100h	[8]
NiCoP@rGO	59	50	18 h at 250 mV static potential	[9]
RuCo alloy	28	31	Not given	[10]
Ru-doped CuO/MoS_2	198	113	15 h	[11]
4H/fcc Ru NTs	23	29.4	Not given	[12]
RuND/C	43.4	49	2.5 h at -0.05 V	[13]
Pd@RuNRs	30	30	12 h at -0,031 V	[14]
$Cu_{2-x}S$@Ru NPs	82	48	12 h at -0.05 V	[15]
Ru_2Ni_2SNs	40	23.4	Not given	[16]
Ru@g-CN_x	53.2	33.2	45 h at -10 mA cm^{-2}	This work

Table S3. *Comparison table of Ru based electrocatalysts for OER in 1M KOH*

Catalyst	Overpotential (At 10mA cm^{-2})	Tafel slope (mV dec^{-1})	Stability	References
0.27-RuO_2@C	250	68	100 h	[8]
Ru_2Ni_2 SNs/C	310	75	Not given	[16]
Ru-doped CuO/MoS_2	201	229	20 h	[11]
NiCoP/rGO	270	65.7	18 h at 50mA cm^{-2}	[9]
RuO_2/N-C	280	56	18h at 1.5 V	[17]
NiFeRu-LDH	225	32.4	10 h at 10 mA cm^{-2}	[18]
$Ni_{1.25}Ru_{0.75}P$	340	Not given	20 h at 1.57 mA cm^{-2}	[19]
$RuIrO_x$	250	50	Not given	[20]
Ru@g-CN_x	280	49.5	45 h at 10 mA cm^{-2}	This work

Table S4. *Comparison table of some excellent electrocatalysts for overall water splitting in 1M KOH*

Catalyst	Electrolyte	Cell voltage (At 10mA cm^{-2})	References
RuCu NSs	1 M KOH	1.49V	[21]
NC-CNT/CoP	1M KOH	1.63 V	[22]
Mo-Co_9S_8@C	1M KOH	1.56V	[23]
Ru-NiFe-P	1M KOH	1.47V	[24]
Co_9S_8–NSC@Mo_2C	1M KOH	1.61	[25]
Pt-CoS_2/CC	1M KOH	1.55	[26]
$RuTe_2$-400	1M KOH	1.57 V	[27]
Ru-NiCoP/NF	1M KOH	1.515 V	[28]
Ru@g-CN_x	1M KOH	1.51V	This work

References:

1. B. B. Beyene, S. B. Mane and C.-H. Hung, *Chemical Communications*, 2015, **51**, 15067-15070.
2. J. Mahmood, F. Li, S.-M. Jung, M. S. Okyay, I. Ahmad, S.-J. Kim, N. Park, H. Y. Jeong and J.-B. Baek, *Nature Nanotechnology*, 2017, **12**, 441-446.
3. J.-Q. Chi, W.-K. Gao, J.-H. Lin, B. Dong, K.-L. Yan, J.-F. Qin, B. Liu, Y.-M. Chai and C.-G. Liu, *ChemSusChem*, 2018, **11**, 743-752.
4. T. Liu, B. Feng, X. Wu, Y. Niu, W. Hu and C. M. Li, *ACS Applied Energy Materials*, 2018, **1**, 3143-3150.
5. Z. Pu, I. S. Amiinu, Z. Kou, W. Li and S. Mu, *Angewandte Chemie International Edition*, 2017, **56**, 11559-11564.
6. S. Liu, Q. Liu, Y. Lv, B. Chen, Q. Zhou, L. Wang, Q. Zheng, C. Che and C. Chen, *Chemical Communications*, 2017, **53**, 13153-13156.
7. Q. Wang, M. Ming, S. Niu, Y. Zhang, G. Fan and J.-S. Hu, *Advanced Energy Materials*, 2018, **8**, 1801698.
8. H.-S. Park, J. Yang, M. K. Cho, Y. Lee, S. Cho, S.-D. Yim, B.-S. Kim, J. H. Jang and H.-K. Song, *Nano Energy*, 2019, **55**, 49-58.
9. J. Li, M. Yan, X. Zhou, Z.-Q. Huang, Z. Xia, C.-R. Chang, Y. Ma and Y. Qu, *Advanced Functional Materials*, 2016, **26**, 6785-6796.
10. J. Su, Y. Yang, G. Xia, J. Chen, P. Jiang and Q. Chen, *Nature Communications*, 2017, **8**, 14969.
11. A. Maiti and S. K. Srivastava, *ACS Applied Nano Materials*, 2021, **4**, 7675-7685.
12. Q. Lu, A.-L. Wang, H. Cheng, Y. Gong, Q. Yun, N. Yang, B. Li, B. Chen, Q. Zhang, Y. Zong, L. Gu and H. Zhang, *Small*, 2018, **14**, 1801090.
13. K. Gao, Y. Wang, Z. Wang, Z. Zhu, J. Wang, Z. Luo, C. Zhang, X. Huang, H. Zhang and W. Huang, *Chemical Communications*, 2018, **54**, 4613-4616.
14. Y. Luo, X. Luo, G. Wu, Z. Li, G. Wang, B. Jiang, Y. Hu, T. Chao, H. Ju, J. Zhu, Z. Zhuang, Y. Wu, X. Hong and Y. Li, *ACS Applied Materials & Interfaces*, 2018, **10**, 34147-34152.
15. D. Yoon, J. Lee, B. Seo, B. Kim, H. Baik, S. H. Joo and K. Lee, *Small*, 2017, **13**, 1700052.
16. J. Ding, Q. Shao, Y. Feng and X. Huang, *Nano Energy*, 2018, **47**, 1-7.
17. C.-Z. Yuan, Y.-F. Jiang, Z.-W. Zhao, S.-J. Zhao, X. Zhou, T.-Y. Cheang and A.-W. Xu, *ACS Sustainable Chemistry & Engineering*, 2018, **6**, 11529-11535.
18. G. Chen, T. Wang, J. Zhang, P. Liu, H. Sun, X. Zhuang, M. Chen and X. Feng, *Advanced Materials*, 2018, **30**, 1706279.
19. D. R. Liyanage, D. Li, Q. B. Cheek, H. Baydoun and S. L. Brock, *Journal of Materials Chemistry A*, 2017, **5**, 17609-17618.
20. Z. Zhuang, Y. Wang, C.-Q. Xu, S. Liu, C. Chen, Q. Peng, Z. Zhuang, H. Xiao, Y. Pan, S. Lu, R. Yu, W.-C. Cheong, X. Cao, K. Wu, K. Sun, Y. Wang, D. Wang, J. Li and Y. Li, *Nature Communications*, 2019, **10**, 4875.
21. Q. Yao, B. Huang, N. Zhang, M. Sun, Q. Shao and X. Huang, *Angewandte Chemie International Edition*, 2019, **58**, 13983-13988.

22. C. Guan, H. Wu, W. Ren, C. Yang, X. Liu, X. Ouyang, Z. Song, Y. Zhang, S. J. Pennycook, C. Cheng and J. Wang, *Journal of Materials Chemistry A*, 2018, **6**, 9009-9018.
23. L. Wang, X. Duan, X. Liu, J. Gu, R. Si, Y. Qiu, Y. Qiu, D. Shi, F. Chen, X. Sun, J. Lin and J. Sun, *Advanced Energy Materials*, 2020, **10**, 1903137.
24. M. Qu, Y. Jiang, M. Yang, S. Liu, Q. Guo, W. Shen, M. Li and R. He, *Applied Catalysis B: Environmental*, 2020, **263**, 118324.
25. X. Luo, Q. Zhou, S. Du, J. Li, J. Zhong, X. Deng and Y. Liu, *ACS Applied Materials & Interfaces*, 2018, **10**, 22291-22302.
26. X. Han, X. Wu, Y. Deng, J. Liu, J. Lu, C. Zhong and W. Hu, *Advanced Energy Materials*, 2018, **8**, 1800935.
27. B. Tang, X. Yang, Z. Kang and L. Feng, *Applied Catalysis B: Environmental*, 2020, **278**, 119281.
28. D. Chen, R. Lu, Z. Pu, J. Zhu, H.-W. Li, F. Liu, S. Hu, X. Luo, J. Wu, Y. Zhao and S. Mu, *Applied Catalysis B: Environmental*, 2020, **279**, 119396.